

# Microbunching Instability Based Synchrotron Radiation Sources

Atoosa Meseck

*Helmholtz-Zentrum Berlin, Germany*

(Dated: April 9, 2021)

Although microbunching-instability (MBI) based synchrotron-radiation facilities do not exist yet, the prominent presence of this space-charge driven instability in the high-brightness accelerator facilities promotes the ongoing worldwide effort to mastering it. Thereby not only the possible countermeasures but also the applications of MBI are in focus of the research. So far, the observed microbunching wavelengths are in IR or optical regime. Shifting the microbunching towards shorter wavelengths seems to require either very high-bunch peak currents or extremely small emittances. These extreme characteristics are difficult to generate and hard to preserve. This letter proposes a novel magnetic device which allows to amplify the initial shot noise at wavelengths in EUV and XUV range with moderate peak current and emittance. It consists of permanent magnets. The specific combination of focusing channels, dispersive chicanes and single focusing elements in this device allows for optimal amplification of microbunching by the longitudinal-space charge-impedance. Extensive simulation studies for different beam energies show the performance of the proposed device, which fed for example with an energy recovery linac can provide ultra-short coherent-high power-radiation pulses with a high repetition rate.

PACS numbers: 41.60 Ap, 41.85Lc, 41.85Ct, 41.75Ht

Similar to the free-electron laser (FEL) instability, the MBI launches out the initial shot noise in the bunch but in contrast to the FEL instability its gain, i.e. the amplification of the microbunching due to the MBI, is not dependent on the radiation field in the undulator. On the one hand, the MBI can cause a significant degradation of the beam quality and is thus a serious threat for example to the performance of an FEL facility. On the other hand as the broadband gain of the MBI is not constrained to the resonant wavelength of the undulator it provides a very attractive alternative for the generation of intense broadband radiation. Accordingly, MBI, possible countermeasures and applications are subject of ongoing research worldwide [1–16].

In order to build a radiation source based on the space-charge driven MBI requires besides a driver accelerator providing a high brightness electron beam a section where the MBI can take place. The beam cross section and divergence as well as the longitudinal dispersion need to be adjusted and controlled along this dedicated section to drive the instability in a controlled manner for a given wavelength range. Throughout the letter, this section will be referred to as the microbunching section. A short undulator tuned to the desired wavelength follows the microbunching section, allowing the microbunched beam to emit high-power radiation. The core piece of such a facility is the microbunching section. The requirements and performance of this section determine the requests on the driver accelerator and the length of the undulator. To identify its requirements and to optimize its performance, one has to examine the emergence of the space-charge driven-microbunching and its amplification.

The MBI has its origin in the longitudinal-space

charge-forces caused by density fluctuations in a relativistic high brightness electron beam. The density fluctuations - i.e. the initial shot noise in the bunch - couple to the bunch's own impedance leading to a longitudinal electrical field (self field), which gives rise to a broadband energy modulation within the same bunch. Dependent on its respective value, the longitudinal dispersion in the accelerator converts this energy modulation into a density modulation, amplifying some of the initial fluctuations while suppressing others. Thus, density modulations within a certain wavelength range are amplified. The process is called microbunching as the beam becomes microbunched at the wavelengths for which the amplitude of the fluctuations are enhanced.

Of course the microbunching is accompanied by an increase of the potential (space-charge) energy of the bunch which needs to be compensated for by the available kinetic energy to obey the energy conservation. For a relativistic bunch passing through an accelerator, the amount of the available kinetic energy depends on the accelerator element. For example in a field free section, i.e. a drift, the available kinetic energy is given by the energy spread of the bunch, while in a magnetic chicane the available energy is amplified proportional to the bending angle squared allowing for a much stronger enhancement of the density modulation [16]. The amplified density modulation in turn leads to a stronger space-charge impedance, causing more energy modulation and thus amplifying further the density modulation in the preferred wavelengths. This way, the space-charge impedance within the bunch drives the microbunching instability.

To design and optimize the microbunching section for wavelengths in EUV and XUV range, one first needs to assess the amount of initial density fluctuations at these wavelengths. For the sake of readability the wavelengths

in EUV and XUV range will be referred to as EUV-wavelengths throughout this document. Due to the finite number of electrons in the bunch, there is a significant amount of noise in transverse and longitudinal electron distribution. The simplified model of the space-charge force – which is frequently used to investigate the microbunching instability in FEL facilities – focuses only on the on-axis longitudinal space-charge field utilizing a one-dimensional model (1D-model)[1–7]. It comprises only the longitudinal fluctuations, leading to a longitudinal electrical field which has its maximum value around a modulation wavelength of  $\lambda_{1D} = 4\pi r_b/\gamma_0$ , where  $r_b$  is the transverse size of the cylindrical bunch,  $\gamma_0$  is the average relativistic factor. For wavelengths shorter than  $\lambda_{1D}$  the field decays with the wavelength squared.

However, transverse density fluctuations can translate into significant fluctuations in the longitudinal electrical field with wavelengths much shorter than  $\lambda_{1D}$  [7–12]. Taking the transverse fluctuations into account, significant density fluctuations for EUV-wavelengths can be expected [12]. The effect of the transverse fluctuations starts to become significant for wavelengths with  $\lambda_{3D} \leq r_b/0.26\gamma_0$  whereby the amplitudes of these fluctuations tend to a constant value independent of the respective wavelength [12].

Space-charge induced MBI at wavelengths shorter than predicted by 1D-model has already been observed [5, 6, 8] confirming thus the validity of the prediction of 3D-model for the density fluctuation at short wavelengths. However, for a dedicated generation of microbunching at a desired EUV-wavelength the existence of corresponding density fluctuations does not suffice. Additionally, a suitable impedance needs to be produced and maintained along the respective microbunching section. A suitable impedance is the impedance which generates the “right” amplitude of the energy modulation leading to the maximum microbunching at the desired wavelength range in connection with the longitudinal dispersion,  $r_{56}$ , of the section.

In the 3D-model the effects of the transverse RMS beam size,  $\sigma_{tra}$ , and divergence,  $\sigma_{tra'}$ , on the microbunching are taken into account. Calculating the bunching factor for a given wavenumber,  $k$ , observed at small angles ( $\theta_x, \theta_y$ ) relative to the longitudinal direction, one obtains for the ensemble average in the 3D-model [9]:

$$\begin{aligned} \langle |b_c(k)|^2 \rangle &\approx \frac{4}{3N} \left( \frac{I_0 r_{56} L_d}{\gamma_0 I_A \sigma_{tra}^2} \right)^2 \\ &\times \frac{\exp\left(-\frac{k^2 r_{56}^2 \sigma_E^2}{2\gamma_0^2} - \frac{k^2 (R_2^2 + \theta_y^2 r_{34}^2) \sigma_{tra'}^2}{2}\right)}{1 + \gamma_0^2 (R_1^2 + \theta_y^2 r_{33}^2)}, \end{aligned} \quad (1)$$

where  $I_0$  is the bunch peak current,  $I_A = 17 \text{ kA}$  is the Alfvén current,  $L_d$  is the length of the microbunching

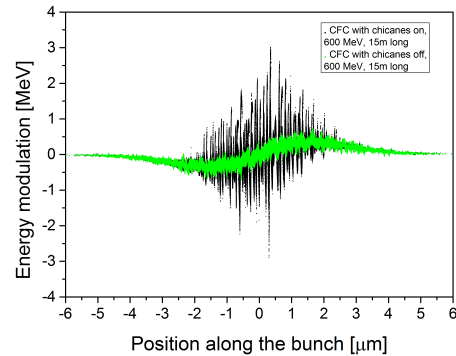


FIG. 1. The MBI-caused energy modulations of 600 MeV bunches in a 15 m long section of compact focusing channel (see Fig. 2) with magnetic chicanes switched on (black dots) and off (green dots).

section,  $\sigma_E$  is the energy spread,  $R_1 = r_{51} + \theta_x r_{11}$ ,  $R_2 = r_{52} + \theta_x r_{12}$ , and  $r_{ij}$  are the elements of the transfer matrix of the microbunching section. The coherent microbunching described in the above formula generates coherent radiation of power:

$$P_{coh} \approx \frac{I_0^2}{4\pi \sigma_{tra}^2} \frac{K^2 L_u^2}{8\gamma_0^2} \langle |b_c(k)|^2 \rangle, \quad (2)$$

in a helical undulator of the length  $L_u$ , where  $Z_0 = 377 \Omega$  is the free space impedance and  $K$  is the undulator parameter. For the maximum bunching, the exponential function in the Eq. 1 has to be adjusted to a value of nearly one. Assuming that the magnetic structure of the microbunching section is such that the two terms in the argument of the exponential function are independent, suitable values for  $r_{56}$  and  $R_2$  can be determined in dependency of the wavelength range, the energy spread and the transverse beam divergence. In principle a FODO lattice with the length  $L$  is an example for such a structure, where  $r_{56} = L/\gamma_0^2$  is independent of  $R_2$ .

However, as a significant enhancement of microbunching requires an enhancement of the available kinetic energy of the bunch [16], the microbunching section needs to contain magnetic chicanes, which shovel effectively a part of the longitudinal momentum of the bunch into the transverse momenta. Figure 1 illustrates the beneficial impact of magnetic chicanes on the energy modulation. Unfortunately magnetic chicanes couple the transverse and longitudinal motion of the particles and thus the respective elements of the transfer matrix, so that in their case  $r_{56}$  and  $R_2$  are not independent anymore.

Considering the above discussion the value of the exponential function in the Eq. 1 can at best be optimized by adjusting the  $r_{56}$  using a magnetic chicane and reducing simultaneously the transverse divergence,  $\sigma_{tra'}$ ,

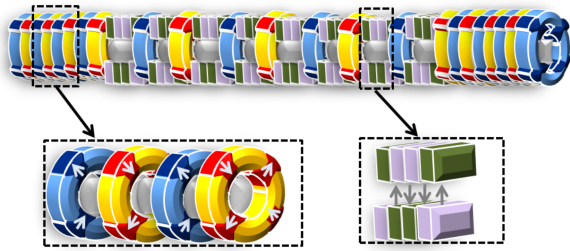


FIG. 2. Schematic view of a CFC piece. The device consists of short permanent magnet quadrupoles (dark blue-blue and red-yellow rings) and dipoles (green-violet blocks), building a combination of pure FODO structures and C-chicane inter-sections.

by reducing the focusing strength in the section which of course leads to an increase of the beam size,  $\sigma_{tra}$ , for a given transverse emittances. Once the  $r_{56}$  and  $\sigma_{tra}$  are fixed, the values of  $I_0$ ,  $\gamma_0$  and  $L_d$  can be adjusted to maximize the first multiplicand in the Eq. 1 in order to maximize the bunching factor. Generally, the beam energy is not a freely-selectable variable because on one hand the longitudinal-space charge-impedance, which drives the MBI, decreases with an increasing beam energy, for bidding too high values of  $\gamma_0$ . On the other hand the beam energy also needs to satisfy the resonance condition of the undulator for a desired EUV-wavelength, thus at least for conventional undulators also low values for  $\gamma_0$  are unfavorable. The length  $L_d$  of the microbunching section is also restricted to a few meters, as  $r_{56} = L_d/\gamma_0^2$  of a longer section smears out the energy modulation before it has a chance to lead to further microbunching amplification in a chicane. Therefore, high-bunch peak currents in combination with very small emittances and energy spreads, i.e. a very high beam brightness seems to be required to drive the MBI. In particular for EUV-wavelengths, this imposes extremely high demands on the accelerator facility.

However, the extreme demands on the accelerator facility can significantly be relaxed by means of a novel magnetic device, which combines in a very compact manner sections of strong-short quadrupole magnets, arranged in dense FODO-structure, with sections of short dipole magnets, arranged in C-chicane structure. The device, called compact focusing channel (CFC), consists of permanent-magnet quadrupoles – for example such as described in [17, 18] with a length of 2-5 cm – and permanent-magnet dipoles of a length of 1-2 cm, providing focusing and bunching in the same device. An schematic view of the CFC is shown in Fig. 2. Similar to undulators also CFCs can be designed for different wavelength ranges, whereby the length of the FODO-structure and chicane sections, the strength of the quadrupoles and dipoles, and the number of magnetic chicanes in the CFC are the properties which have to be designed and opti-

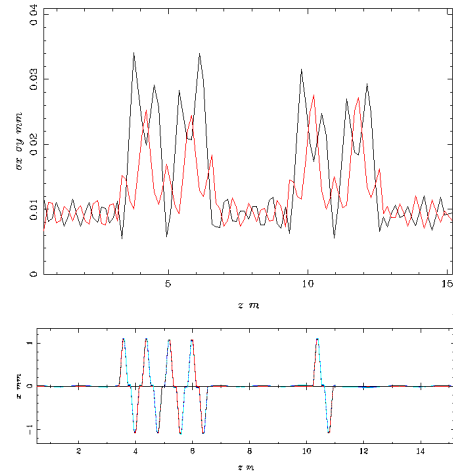


FIG. 3. An example for the development of the transverse beam sizes (top) and beam trajectory (bottom) along a 15 m long section of CFC optimized for EUV-wavelengths is shown.

mized. Also the impact of the coherent synchrotron radiation (CSR) [19] on the microbunched beam has to be taken into account for an optimal design of the chicane sequence. A fine tuning of the quadrupole and dipole strengths of an existing CFC is possible for example by moving the magnets towards the beam axis or further out [20]. Figure 3 shows the development of the beam size and beam trajectory along a 15 m long section of a CFC optimized for the EUV-wavelengths. While the FODO-structure provides a small average beam size of about  $10 \mu\text{m}$ , a sequence of chicanes provide the necessary  $r_{56}$  of about a few hundred  $\mu\text{m}$ . Thereby, the quadrupoles inside the chicane sequence ensure that the  $\sigma_{tra}$  is small in this section. The CFC has a circular aperture of 8 mm in this case.

To investigate the performance of the CFC for EUV-wavelengths extensive simulation studies have been carried out utilizing the 3D-space charge-code ASTRA [21]. In the simulations electron bunches with two different charges of 3.6 pC and 5.1 pC, three different beam energies of 400 MeV, 600 MeV and 900 MeV, two different emittances of 0.1 mm mrad and 0.4 mm mrad – leading to different average transverse beam sizes of  $14 \mu\text{m}$  and  $7 \mu\text{m}$  –, and two energy spreads of 10 keV and 15 keV (for 900 MeV cases) with always the same RMS bunch length of  $1.5 \mu\text{m}$  are modeled using always 200000 macroparticle generated by ASTRA generator. The bunches are tracked through a 15 m long CFC where the 3D-FFT algorithm of ASTRA with a dense grid of 1024 longitudinal and 64 transverse grid cells is used. Generally, the usage of macroparticles reduces the CPU requirements, however it also leads to an artificially increased initial shot noise amplitude, so that the CFC length needed for a desired bunching factor is shorter than in a real facility. This can easily be amended by lengthening the device

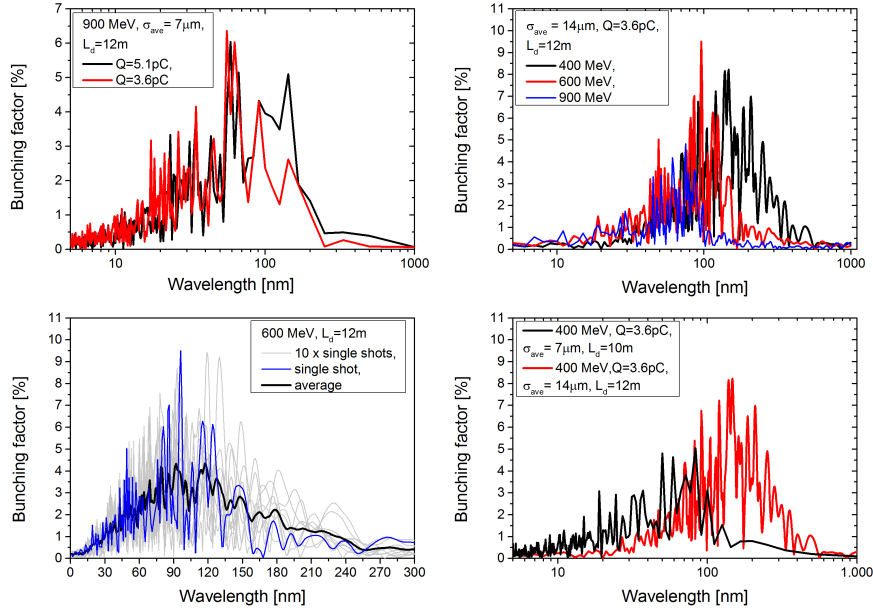


FIG. 4. Bunching factor as a function of wavelength is shown for different beam properties and CFC settings. The bunching factor for 10 consecutive shots is shown in the lower-left graph. For these simulations the average beam size in the CFC was adjusted to  $14\ \mu\text{m}$ . A reduction of the transverse beam size shifts the bunching towards shorter EUV-wavelengths but it also can decrease the maximum value of the bunching as shown in lower-right graph. Also an increase of the bunch charge does not automatically increase the bunching factor for short wavelengths as shown in upper-left graph for 900 MeV bunches. The impact of the beam energy of the bunching factor is depicted in the upper-right graph.

suitably. Using formulas presented in [19], the increase of the energy spread due to the CSR can be calculated. Due to the very low bunch charges, the relative energy deviation generated by CSR in the chicane sections is on the order of  $10^{-5}$  and thus almost two orders of magnitude smaller than the generated energy modulation on the order of  $10^{-3}$  (see Fig. 1).

Figure 4 illustrates the main findings of the simulation studies. As expected starting from shot noise, the MBI shows statistical characteristics clearly visible in the fluctuation of the bunching factor ( Fig. 4 lower-left graph). A reduction of the transverse beam size shifts not only the bunching towards shorter wavelengths but also decreases the value of the exponential function in Eq. 1 so that in spite of the increase in the first multiplicand of the equation the bunching factor itself is lower for the smaller beam size as shown for 400 MeV bunches in Fig. 4 ( lower-right graph). Also an increase of the bunch charge does not automatically increase the bunching factor for EUV-wavelengths, as it also drives an increase in the longitudinal beam size which can dominate leading thus to an enhancement of the bunching for longer wavelengths as shown in Fig. 4 (upper-left graph). Generally, the beam energy and bunch charge are powerful knobs to adjust the bunching factor for an existing CFC. The impact of the beam energy of the bunching factor is depicted in

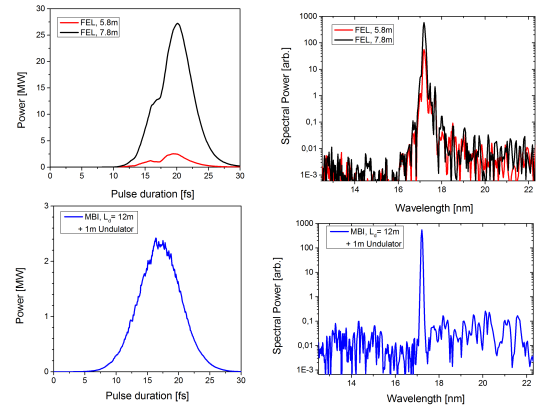


FIG. 5. Comparison of simulated radiation power and spectral power profile for an FEL and a MBI microbunched undulator output.

Fig. 4 (upper-right graph). An increase of beam energy shifts the bunching towards shorter wavelength but it also decreases the amplitude of the bunching factor.

From Eq. 2 one expects high-coherent radiation-power generated by a microbunched beam in a 1 m long helical undulator. In order to verify this expectation and to study the spectral properties of the radiation gener-

ated by a MBI based source, the output of a 900 MeV ASTRA-run ( $7\ \mu\text{m}$ -3.6 PC case in Fig. 4 upper-left graph) is used as an input for coherent radiation simulation, where the 3D-FEL code GENESIS [22] is utilized. For comparison also FEL simulations with the initial, i.e. pre-microbunching, bunch are performed. Figure 5 shows the comparison. The MBI-based radiation source has a bandwidth smaller than the FEL source. After 5.8 m the FEL generates radiation with the same peak power as the MBI source in 1 m [23]. After 7.8 m the FEL reaches the same spectral power. The slight shoulder in the FEL power profile (Fig. 5 (upper-left graph)) is caused by a combination of the slippage and the very short bunch length. It translates into additional spectral width, limiting the minimum spectral bandwidth of the FEL for bunch lengths shorter than slippage. The pulse generated by a MBI based source does not suffer from this effect and thus shows a Fourier transform limited bandwidth.

CFC devices proposed in this letter allows one to drive the MBI in a desired wavelength range most efficiently. Thus, they have the potential to be the core piece of MBI-based synchrotron-radiation sources. Simulation studies presented prove that utilizing a CFC fed by a high brightness accelerator and followed by a short undulator, short (femtosecond long) radiation pulses in EUV range with spectral properties better than the FEL can be generated. Using CFCs in high repetition rate accelerators (with GHz rate) allow for the generation of high average power by the subsequent undulator. The combination of high brightness, high repetition rate and low bunch charge hints in direction of energy recovery linacs as most the suitable accelerators for driving CFC based sources. The proposed CFC devices can also amplify a microbunching imprinted to the bunch by seeding in a prior undulator, thus it can also assist the FEL process. Furthermore, CFCs can be envisaged as microbunching-amplifiers in electron cooling schemes at colliders [24].

The author would like to thank A. Gaupp and R. Mitzner for their insightful comments.

- 
- [1] M. Borland, Y. C. Chae, P. Emma, J. W. Lewellen, V. Bharadwaj, W. M. Fawley, P. Krejcik, C. Limborg, S. V. Milton, H.-D. Nuhn, R. Soliday, and M. Woodley, Nucl. Instrum. Methods Phys. Res. A **483**, 268 (2002).  
 [2] E. L. Saldin, E. A. Schneidmiller, and M. V. Yurkov, Nucl. Instrum. Methods Phys. Res. A **490**, 1 (2002).

- [3] S. Heifets, G. Stupakov, and S. Krinsky, Phys. Rev. ST Accel. Beams **5**, 064401 (2002).  
 [4] Z. Huang and K.-J. Kim, Phys. Rev. ST Accel. Beams **5**, 074401 (2002).  
 [5] Z. Huang, M. Borland, P. Emma, J. Wu, C. Limborg, G. Stupakov, and J. Welch, Phys. Rev. ST Accel. Beams **7**, 074401 (2004).  
 [6] T. Shafiq and Z. Huang, Phys. Rev. ST Accel. Beams **7**, 080702 (2004).  
 [7] M. Venturini, Phys. Rev. ST Accel. Beams **10**, 104401 (2007).  
 [8] E. L. Saldin, E. A. Schneidmiller, and M. V. Yurkov, Nucl. Instrum. Methods Phys. Res. A **528**, 355 (2004).  
 [9] D. Ratner, A. Chao, and Z. Huang, in *FEL Conference* (Gyeongju, Korea, 2008) pp. 338–341.  
 [10] A. Gover and E. Dyumin, Phys. Rev. Lett. **102**, 154801 (2009).  
 [11] H. Loos, R. Akre, A. Brachmann, F.-J. Decker, Y. T. Ding, D. Dowell, P. Emma, J. C. Frisch, A. Gilovich, G. R. Hays, P. Hering, Z. Huang, R. H. Iversen, C. Limborg-Deprey, A. Miahnahri, S. Molloy, H.-D. Nuhn, J. L. Turner, J. J. Welch, W. E. White, J. Wu, and D. F. Ratner, in *FEL Conference* (Gyeongju, Korea, 2008) pp. 485–489.  
 [12] M. Venturini, Phys. Rev. ST Accel. Beams **11**, 034401 (2008).  
 [13] A. Marinelli and J. B. Rosenzweig, Phys. Rev. ST Accel. Beams **13**, 110703 (2010).  
 [14] E. A. Schneidmiller and M. V. Yurkov, Phys. Rev. ST Accel. Beams **13**, 110701 (2010).  
 [15] A. Marinelli, E. Hemsing, M. Dunning, D. Xiang, S. Weathersby, F. O’Shea, I. Gadjev, C. Hast, and J. B. Rosenzweig, Phys. Rev. Lett. **110**, 264802 (2013).  
 [16] V. Litvinenko and G. Wang, in *FEL Conference* (BASEL, Swiss, 2014).  
 [17] T. Eichner, F. Grüner, S. Becker, M. Fuchs, D. Habs, R. Weingartner, U. Schramm, H. Backe, P. Kunz, and W. Lauth, Phys. Rev. ST Accel. Beams **10**, 082401 (2007).  
 [18] S. Becker, M. Bussmann, S. Raith, M. Fuchs, R. Weingartner, P. Kunz, W. Lauth, U. Schramm, M. El Ghazaly, F. Grüner, H. Backe, and D. Habs, Phys. Rev. ST Accel. Beams **12**, 102801 (2009).  
 [19] E. L. Saldin, E. A. Schneidmiller, and M. V. Yurkov, Nucl. Instrum. Methods Phys. Res. A **398**, 373 (1997).  
 [20] J. Bahrtdt, “Private communication,” HZB, Berlin (2014).  
 [21] K. Flöttmann, *ASTRA: A Space Charge Tracking Algorithm*, DESY, Hamburg, [www.desy.de/~mpyf10](http://www.desy.de/~mpyf10) (2000).  
 [22] S. Reiche, Nucl. Instrum. Methods Phys. Res. A **429**, 243 (1999).  
 [23] Of course for a calculation of total length and cost, the 12 m CFC needed to produce the bunching has been taken into account.  
 [24] D. Ratner, Phys. Rev. Lett. **111**, 084802 (2013).